EFDA–JET–PR(11)53

Y. Sun, Y. Liang, K.C. Shaing, Y. Q. Liu, H.R. Koslowski, Jachmich, B. Alper, A. Alfier, O. Asunta, P. Buratti, G. Corrigan, E. Delabie, C. Giroud, M.P. Gryaznevich, D. Harting, T. Hender, E. Nardon, V. Naulin, V. Parail, T. Tala, C. Wiegmann, S. Wiesen, T. Zhang and JET EFDA contributors

Non-Resonant Magnetic Braking on JET and TEXTOR

Non-Resonant Magnetic Braking on JET and TEXTOR

Y. Sun[1,2], Y. Liang[1], K.C. Shaing[3,4], Y. Q. Liu[5], H.R. Koslowski[1], Jachmich[6], B. Alper[5], A. Alfier[7], O. Asunta[8], P. Buratti[9], G. Corrigan[5], E. Delabie[1], C. Giroud[5], M.P. Gryaznevich[5], D. Harting[1], T. Hender[5], E. Nardon[10], V. Naulin[11], V. Parail[5], T. Tala[12], C. Wiegmann[1], S. Wiesen[1], T. Zhang[1] and JET EFDA contributors*

JET-EFDA, Culham Science Centre, OX14 3DB, Abingdon, UK

[1]Institute for Energy and Climate Research - Plasma Physics, Forschungszentrum Jülich, Association EURATOM-FZJ, Trilateral Euregio Cluster, 52425 Jülich, Germany
[2]Institute of Plasma Physics, Chinese Academy of Sciences, PO Box 1126, Hefei 230031, Peoples Republic of China
[3]Institute for Space, Astrophysical and Plasma Sciences, National Cheng Kung Unversity, Tainan, Taiwan 70101, Republic of China
[4]Engineering Physics Department, University of Wisconsin, Madison, WI 53706, USA
[5]EURATOM-CCFE Fusion Association, Culham Science Centre, OX14 3DB, Abingdon, OXON, UK
[6]Association EURATOM-Belgian State, Koninklijke Militaire School-Ecole Royale Militaire, B-1000 Brussels, Belgium
[7]Associazione EURATOM-ENEA sulla Fusione, Consorzio RFX Padova, Italy
[8]Association EURATOM-Tekes, Aalto University, P.O.Box 14100 FI-00076 AALTO, Finland
[9]Associazione EURATOM-ENEA sulla Fusione, C.R. Frascati, CP65, 00044 Frascati, Italy
[10]CEA/IRFM Cadarache, F-13108, St. Paul-lez-Durance, France
[11]Association EURATOM-Risφ National Laboratory, OPL-128 Risφ, DK-4000 Roskilde, Denmark 12 Association EURATOM-Tekes, VTT, P.O. Box 1000, FIN-02044 VTT, Finland
** See annex of F. Romanelli et al, "Overview of JET Results", (23rd IAEA Fusion Energy Conference, Daejon, Republic of Korea (2010)).*

Preprint of Paper to be submitted for publication in
Nuclear Fusion

ABSTRACT.
The non-resonant magnetic braking effect induced by an non-axisymmetric magnetic perturbation is investigated on JET and TEXTOR. The collionality dependence of the torque induced by the n = 1, where n is the toroidal mode number, magnetic perturbation generated by the error field correction coils on JET is observed. The observed torque is located mainly in the plasma core (normalized radius $\rho < 0.4$) and increases with decreasing collisionality. The neoclassical toroidal plasma viscosity torque in collisionless regime is modeled by using the numerical solution of the bounce averaged drift kinetic equation. The calculated collisionality dependence of the neoclassical toroidal plasma viscosity torque is in good agreement with the experimental observation on JET. The reason for this collisionality dependence is that the torque in the plasma core on JET mainly comes from the flux of the trapped electrons, which are still mainly in the $1/\nu$ regime. The strongest neoclassical toroidal plasma viscosity torque torque on JET is also located near the plasma core. The magnitude of the neoclassical toroidal plasma viscosity torque strongly depends on the plasma response, which is also discussed in this paper. There is no obvious braking effect with n = 2 magnetic perturbation generated by the dynamic ergodic divertor on TEXTOR, which is consistent with the neoclassical toroidal plasma viscosity modeling.

1. INTRODUCTION

The magnetic field of a tokamak is designed to be toroidally symmetric. Realistically, there is always a slight Non-Axisymmetric Magnetic Perturbation (NAMP) due to an intrinsic error field, MagnetoHydroDynamic (MHD) perturbations in the plasma or external magnetic perturbations applied to control Edge Localized Modes (ELMs) [1, 2] and Resistive Wall Modes (RWMs) [3]. The magnetic braking effect without mode locking during the application of NAMP has been observed in tokamak experiments [4, 5, 6, 7, 8]. It was named as non-resonant magnetic braking to distinguish to the resonant braking during the mode locking phase. Because of the importance of the plasma rotation, it is necessary to understand the mechanism of this braking effect.

In a low collisionality plasma, breaking of the toroidal symmetry will result in a so-called Neoclassical Toroidal plasma Viscosity (NTV) [9] torque. The NTV torque is a potential explanation of the observed braking effect [4, 5, 8].

A good agreement between the calculated NTV torque in the $1/\nu$ regime and the observed one induced by the applied NAMP has been reported from NSTX [4]. Here, ν is the collisionality. The collisionality dependence of the braking effect on NSTX was also consistent with the NTV torque in the $1/\nu$ regime [7]. The so-called steady-state flow [9] or 'off-set' rotation [10] predicted from the NTV theory has been observed on DIII-D [5]. On DIII-D, the calculated NTV damping time in the ν regime was about two orders longer than the observation [11]. The MHD induced braking effect on MAST was in agreement with the NTV theory in the $1/\nu$ regime [12]. A strong non-resonant magnetic braking effect has been observed in ELM control experiments with n = 1 NAMP field generated by the Error Field Correction Coils (EFCCs) on JET [13, 8]. The observed

torque was mainly located in the plasma core and it was about half of the Neutral Beam Injection (NBI) torque on JET [8]. The magnitude of the observed torque is between the torque predicted by the NTV theory in the $\nu - \sqrt{\nu}$ [14] and $1/\nu$ regimes.

The experimental regime in present tokamaks as well as ITER [11] covers all the $1/\nu$ [9], $\nu - \sqrt{\nu}$ [14] and the superbanana plateau [15] regimes and the transitions between them. Furthermore, particles with different energy are in different collisionality regimes. In order to model the influence on the toroidal plasma rotation with NAMP and compare it with the observation, we need to know the NTV solution in the transitions, as well as in the asymptotic limits of these collisionless regimes.

One approximate analytic general expression of NTV torque has been obtained by smoothly connecting the formula in these different regimes [16]. Another general analytic result has been obtained by using the simple Krook collisional operator [17]. Recently, a numerical solution with the pitch angle scattering collisional operator is obtained by solving the bounce averaged drift kinetic equation [18, 19]. The numerical solution is valid for all these important regimes and their transitions. A good agreement between the smoothly connected formula and the numerical solution in different asymptomatic limits has been obtained, while there were some differences at the transition regimes as expected [18, 19]. The refinement of the analytic formula can improve the agreement between the analytic solution and the numerical solution [20, 21].

In this paper, the non-resonant magnetic braking effect induced by the NAMP on JET and TEXTOR are investigated and compared with the NTV theory. This paper is organized as follows. The experimental observations are presented in section 2. The NTV torque evaluation and the comparison with the observations are discussed in section 3, followed by the summary of the main results in section 4.

2. EXPERIMENTAL OBSERVATIONS

2.1. Collisionality dependence of the braking effect by n = 1 NAMP on JET

The Error Field Correction Coils (EFCCs) on JET are shown in Fig.1. Each coil has 16 turns. They are located outside the vacuum vessel. It has been frequently used for Edge Localized Modes (ELMs) control on JET [2, 13, 22].

The strength of the n = 1 component of the Resonant Magnetic Perturbation (RMP) spectrum $(b^{\rho}/B^{\zeta})_{mn}$ (%) in Hamada coordinates of the applied NAMP is shown in the contour plot in Fig.2. The vertical axis is the radial position and the horizontal axis is the poloidal mode number m. The radial coordinate $\rho = \sqrt{\psi_T/\pi B_0}$ is used in this paper (Normalized ρ, with $\rho = 1$ at the last close surface, is used in all the figures). Here ψ_T is the toroidal magnetic flux and B_0 is the magnetic field strength at the magnetic axis. The dashed line indicates the resonance condition m = nq at different radii, and the shot solid lines mark the locations and widths of the islands induced by the NAMP using the vacuum field assumption. There is a small n = 3 harmonic in this coil configuration. Because the coils are located outside the vacuum vessel, the magnetic perturbation has a slow decay along the minor radius and is also quite strong near the plasma core.

A density pump out usually occurs in ELM control experiment by the application of a low n NAMP field on JET [13]. Recently, the plasma density drop during the application of NAMP field was compensated by gas puffing (JET Pulse No: 77334 as shown in Fig.3) or pellet injection (JET Pulse No's: 77328, 77331, 77333 and 77337 as shown in Fig.). The equilibrium configuration of these pulses were kept the same. The plasma collisionality changed a lot when the plasma density was restored at different levels.

Figure 3 shows the temporal evolution of the plasma rotation (A), density (B), ion temperature (C) at $R_0 = 3.0$m (near the magnetic axis) during the application of n = 1 NAMP field (D) for a series of pulses, in which the densities were restored at different levels.

In these pulses, the toroidal magnetic field strength is $B_0 = 1.8$T, the injected beam power is 10.5MW and the safety factor q at $\hat{\psi}_p = 0.95$ is $q_{95} = 3.2$. Here, $\hat{\psi}_p$ is the normalized poloidal magnetic flux. After the NAMP field is applied, the plasma core rotation for each pulse dramatically reduces to about half of its initial rotation without NAMP. There is no mode locking observed in these pulses.

Among these pulses the effective ion collisionalities $\nu_{*,i} \equiv \nu_i/(\in^{3/2}\omega_{ti})$ near the plasma core region are changed by about one order which is shown in Fig.4. Here νi is the ion collisionality, $\omega_{ti} = v_{ti}/qR_0$ is the ion transient frequency and v_{ti} is the ion thermal velocity.

The torque density profiles induced by the n = 1 NAMP at t = 23s are calculated by momentum transport analysis [8] and are shown in Fig.5. The maximum torque is located at the plasma core region, which is similar to the previous observation [8].

The obtained torque profiles obviously depend on the collisionality. The collsionality dependence of the total torque inside the $\rho = 0.4$ is shown in Fig.6. The torque increases with decreasing collisionality, which is similar to the dependence observed on NSTX [7].

2.2. NON-RESONANT MAGNETIC BRAKING EXPERIMENT WITH N = 2 DED ON TEXTOR

The non-resonant magnetic braking induced by the Dynamic Ergodic Divertor (DED) [23], shown in Fig.7, in n = 2 configuration on TEXTOR is investigated. The DED is an in-vessel coil system and is similar to the helical winding coils with fixed magnetic pitch.

The strength of the n = 2 component of the RMP spectrum of the coil configuration is shown in Fig.8. Compared to the spectrum of the n = 1 NAMP on JET, the perturbation field decayed quickly along the minor radius from the plasma edge to the core. There is an asymmetry on the poloidal mode number in the spectrum because of the fixed pitch angle in the perturbation field. By changing the orientation of the plasma current with fixed orientation of the toroidal field, the spectrum of the perturbation can be resonant ($m < 0$) or non-resonant($m > 0$) dominant case. The sign of the poloidal mode number comes from the convention in the definition of the coordinates.

The evolution of the toroidal angular momentum density near the plasma core for these two configurations with the DED coil current is shown in Fig.9. No obvious braking effect is observed

with this coil configuration for both resonant (solid line) and non-resonant (dashed line) cases. For the resonant dominant case, there is an acceleration effect, which may be due to the formation of stochastic field near the plasma edge and has been reported before [24].

3. MODELLING THE NEOCLASSICAL TOROIDAL PLASMA VISCOSITY (NTV) TORQUE AND COMPARING IT WITH THE OBSERVED TORQUE

In collisionless plasma, the breaking of the toroidal symmetry due to the NAMP can cause additional radial drift of the trapped particles, and hence a radial neoclassical transport. This effect on ion and electron are often different, which means non-ambipolar transport. To satisfy the ambipolarity condition, the radial electric field need to be modified. Therefore, it is equivalent to a torque to change the plasma rotation. This toroidal torque is represented as a toroidal viscosity, which is called neoclassical toroidal plasma viscosity [9].

The toroidal drift of the particles has an effect to reduce this transport. Therefore, the results can be further divided into different regimes, depending on the magnitude of the $\vec{E} \times \vec{B}$ drift and the ∇B drift compared to the collisionality. They have been summarized in [16]. Of all these regimes, the most important regimes for tokamak with small perturbation are the $1/\nu$ regime [9], the $\nu - \sqrt{\nu}$ regime [14] and the superbanana plateau regime [15].

We employ the numerical model developed in [18, 19] to calculate the NTV torque density profile. The model is valid for the most important regimes and their transitions. In different asymptotic limits, it can well reproduce the results from the analytic solution. As expected, the results had some differences at the transition regimes, compared to that from the connected formula [16]. It has been discussed before in details in [19].

3.1. NTV TORQUE DENSITY

The magnetic field in tokamaks can be expressed as

$$\vec{B} = \frac{d\psi_p}{d\hat{V}} \nabla \hat{V} \times \nabla \alpha = \nabla \phi \times \psi_p + g\,(\psi)\, \nabla \phi \tag{1}$$

where $-2\pi\psi_p$ is the poloidal magnetic flux, $\hat{V} \equiv V/(4\pi^2)$, V is the plasma volume enclosed by the flux surface and $\alpha = q\theta - \zeta$ is the drift angle, ϕ is the geometric toroidal angle, $g = RB_t$ and B_t is the toroidal magnetic field.

$(\hat{V}, \theta, \zeta)$ are the Hamada coordinates with Jacobin $J = 1$. Therefore, the Jacobin of (ρ, θ, ζ) becomes $\hat{J} = V' = \rho B_0/(g < 1/R^2 >_\psi)$, where the prime denotes the derivative over ρ and $< ... >_\psi$ denotes flux surface average.

The magnetic field strength with NAMP can be written as,

$$B = B_0 \left[1 - \epsilon \cos\theta - \sum_n b_n(\theta) e^{in\alpha}\right] \tag{2}$$

where $\in \approx r/R$ is the amplitude of the $\cos\theta$ component of the equilibrium field caused by toroidicity, r and R are the minor and major radius, respectively, $b_n = \Sigma_m b_{mn} e_{i(m-nq)\theta}$ is the n_{th} Fourier harmonic of the perturbation field and bmn are the Fourier coefficients of $\delta B/B_0$ in(θ,ζ) coordinates on the distorted flux surfaces [9].

According to the results in [18, 19], the NTV torque density can be evaluated from

$$T_{NTV} = -\tau_{NTV}^{-1} L_\phi \tag{3}$$

where $L_\phi \equiv \rho_i \langle R^2 \rangle_\psi \omega_\phi$ is the toroidal angular momentum density, $\rho_i = M_i N_i$ is the ion mass density, and

$$\tau_{NTV}^{-1} = \frac{R_0^2}{\langle R^2 \rangle_\psi} \sum_{j=i,e} \sum_n \frac{\sqrt{\in}\, q^2 \omega_{ti}^2}{2\sqrt{2}\pi^{3/2}} \left| \frac{e_i}{e_j} \right| \times \lambda_{1,n} (1 - \omega_{nc,n}/\omega_\phi) \tag{4}$$

$$\omega_{nc,n}^j \equiv q(\omega_\theta + \omega_{*,j} - \omega_{*,i} + \frac{\lambda_{2,n}}{\lambda_{1,n}} \omega_{*T,i}) \tag{5}$$

$$\lambda_{1,n} \equiv \frac{1}{2} \int_0^\infty I_{\kappa n}(x)(x - 5/2)^{l-1} x^{5/2} e^{-x} dx \tag{6}$$

where ω_ϕ and ω_θ are the toroidal and poloidal angular frequencies, $\omega_* \equiv P'/(\rho B_0 eN)$ and $\omega_{*T} \equiv T'/(\rho B_0 e)$ are the diamagnetic frequencies. Here the contributions from both trapped ion and electron are included. The NTV torque from the trapped electron is possibly dominant [19]. However, this part was normally neglected in the previous studies.

The energy dependence of pitch angle integral, Iκn, is taken into account in this model. The names of the different regimes essentially come from the collisionality dependence of the pitch angle integral, which can be evaluated from both analytic and numerical solutions [18, 19].

3.2. VARIATION OF THE MAGNETIC FIELD STRENGTH

Before we calculate the NTV torque, we need to evaluate the spectrum of the variation of the magnetic field strength on each flux surface. This is another difficulty in the NTV modeling, besides the complexity of the NTV theory itself.

The variation of the magnetic field strength on the distorted flux surface (or the Lagrangian variation) due to the NAMP $\vec{b}$ can be written as [25, 9, 8],

$$\delta B = \vec{b} \cdot (\vec{B}/B) + (\vec{\xi} \cdot \nabla B) \tag{7}$$

where ξ is the displacement induced by the NAMP. The first term is the so called Eularian part and the second term comes from the displacement of the magnetic flux surface [25]. The second term is normally the dominant one [25, 8].

The NTV theory is based on the existence of closed flux surfaces. For island case, it is well

defined outside the island separatrix, where the closed flux surface still exists [26].

From $\vec{B}_{eq} \cdot \nabla\vec{\xi} = \vec{b}$, the spectrum of the displacement can be written as,

$$\vec{\xi}_{mn} = q\frac{(\vec{b}/B^{\zeta})_{mn}}{i(m - nq)} \tag{8}$$

where $\vec{B}_{eq} = B^{\theta}\vec{e}_{\theta} = (B^{\zeta}/q)e\theta$ is the original two-dimensional equilibrium field.

For resonant case, there are singularities at the rational surfaces $q_s = m/n$, if $(b/B^{\zeta})_{mn}|q_s \neq 0$, i.e. the existence of island. These singularities can be removed by changing $1/(m - nq)$ to $(m - nq)/[(m-nq)^2 + \delta^2_{mn}]$,which is similar to the method used in [25]. The small parameter δ_{mn} can be chosen as $\delta_{mn} = nw_{mn}q'|q_s/2$, where $w_{mn} = 4\sqrt{q(b^{\rho}/B^{\zeta})_{mn}/nq'|q_s}$ is the island width.

The calculation of the displacement of the magnetic flux surface is essentially the same process as the modeling of the plasma response to the magnetic perturbation [27, 28, 11, 29, 30, 31]. How to accurately model the realistic plasma response is still an open question.

In this paper, we use two ways to evaluate the displacement. One way is based on the vacuum field assumption which was often used in the previous analysis. It is equivalent to assume that the perturbed current inside the plasma induced by the plasma response is completely damped away by the plasma resistivity. Therefore, it is a plasma response with infinity resistivity. Another way used in the following is to evaluate the displacement from the linear plasma response model by solving the MagnetoHydrodynamics (MHD) Equations with finite resistivity and plasma rotation from the MARS-F code [30, 31]. The results from this model were in good agreement with the magnetic measurements on DIII-D [32].

3.3. NTV MODELING AND COMPARISON ON JET

The profiles of the normalized collsionalities for JET Pulse No: 77329 are shown in Fig.10. It is shown that it is in the collisionless regime ($\nu_* < 1$) for both electron and ion in most plasma region. For the particles with the normalized energy $x = v^2/v^2$ close to 1, $\nu_{*d0} \equiv \frac{\nu/(2\epsilon)}{|n\omega_{d\alpha}|} = 1$ is defined as the the transition between the $1/\nu$ regime and the $\nu - \sqrt{\nu}$ regime (or the superbanana plateau regime, if $x > x_{min} \equiv |q\omega_E/\omega_{B0}|$). It can be found that the electron is in the $1/\nu$ regime, but close to the transition to the $\nu - \sqrt{\nu}$ regime or the superbanana plateau regime. From $\nu_{*d0,i} < 1$ and the profiles of the xmin shown in Fig.11, the ion are mainly in the $\nu - \sqrt{\nu}$ regime. Near the plasma core, x_{min} is close to 1. Therefore, the superbanana plateau regime is also important for trapped ion near the plasma core. In this case, the NTV from the trapped electron is possibly to be dominant [19]. This part was normally neglected in the previous studies. However, it will be shown in the following that this part in the plasma core is indeed dominant.

The calculated NTV torque density profiles are shown in Fig.12. Here, the variation of the magnetic field strength Eq. (7) is evaluated with the perturbation field $\vec{b}$ calculated using the vacuum field assumption. For the variation of the magnetic field strength, the Eulerian part is around 1 order smaller than the displacement part. Therefore, the NTV torque mainly comes from the displacement

of the flux surfaces. The fundamental harmonic n = 1 gives the dominant contribution in the NTV torque as discussed before [8]. It shows that the strongest contribution is also near the plasma core ($\rho < 0.4$). This is consistent with the observations.

The comparison of the total observed torque and the NTV torque inside the $\rho = 0.4$ surface is shown in Fig.13. The NTV torque shows the same tendency as the observed torque. However, the magnitude of the NTV torque is about one order larger than the observed one.

The NTV torque densities from the different species are shown in Fig.14. It is shown that the torque density from the trapped electrons is about one order larger than that from the ions near the plasma core. Because the trapped electron is still in the $1/\nu$ regime, the NTV torque also increases with decreasing collisionality, which is consistent with the observed torque dependence on JET.

3.4. INFLUENCE OF THE PLASMA RESPONSE

In the above analysis, we have used the vacuum field assumption, which resembles to the infinite resistivity plasma response. However, the realistic plasma resistivity is finite. Depending on the plasma β and mode number, the perturbation field may be shielded or amplified by the perturbed current generated inside the plasma. The Resonant Field Amplification (RFA) effect is not important in the target plasma chosen in this experiment [33]. However,the perturbation field may be shielded by the plasma response because of the plasma rotation.

The MARS-F code [30, 31] is employed to model the linear MHD plasma response with finite resistivity and plasma rotation. The advantage of this code is that it takes full toroidal geometry, and hence the toroidal coupling effect of the harmonics with different poloidal mode number is included. The disadvantage of this code is that the resistivity and the perpendicular viscosity are not self-consistently modeled, but they are input parameters. The importance of the kinetic effect in the plasma resistivity is shown in [27].

The plasma response from the MHD response strongly depends on the plasma resistivity and rotation [30]. The effect of the plasma resistivity is taken into account via the Lundquist number $S \equiv \tau_R/\tau_A$, where τ_R and τ_A are the resistive diffusion time and the Alfv ´en time, respectively. The radial profile of the Lundquist number $S = S_0(T_e/T_{e0})^{3/2}$ is used in the modeling [31]. Here the subscript 0 denotes the value at the magnetic axis. The typical Lundquist number at the magnetic axis, S_0 is of the order 10^8 using the neoclassical resistivity calculated from the Spitzer formula.

The spectrum of the magnetic perturbation with plasma response for $S_0 = 0.8 \times 10^8$ is shown in Fig.15. The resonant magnetic perturbation with $|m - n_q| \approx 0$ is strongly shielded. There is no q = 1 surface in this equilibrium. Therefore, the plasma response to the m/n = 1/1 component near the plasma core is caused by the mode coupling of the global n = 1 mode. There are also some non-resonant harmonics with $|m - n_q| \geq 1$ that can be amplified, similar to the previous results shown in [30].

Because the NTV torque mainly comes from the nearest resonant harmonic (or minimum value of $\delta \equiv |m - n_q|$) [19], the m/n = 1/1 harmonic gives the dominant contribution near the plasma core.

The m/n = 1/1 component of the radial displacements calculated using the vacuum field assumption and the MHD response are shown in Fig.16. The m/n = 1/1 displacement near the plasma core evaluated using the vacuum field assumption is very large, because there is a strong m/n = 1/1 magnetic perturbation and the central q value is very close to 1 and flat (dashed line shown in Fig.2 or Fig.17 (A)). The profile of the m/n = 1/1 displacement calculated using the MHD response is similar to the internal kink, and the amplitude strongly depends on the plasma resistivity. For the lower resistivity case ($S_0 = 5.3\times 10^8$, dashed dotted), the m/n = 1/1 displacement is strongly reduced compared to that in the vacuum field case (triangles). For the higher resistivity case ($S_0 = 0.53 \times 10^8$, solid), it is close to the level in the vacuum case.

The Poincaré plots of the magnetic field with the plasma response for different S_0 as well as with the vacuum field assumption shown in Fig.17 confirm the differences in the radial displacement near the plasma core for these cases.

The NTV torque density with the variation of the magnetic field strength evaluated from the MHD response (dashed line) for JET Pulse No: 77329 is shown in Fig.18. For $S_0 = 1.1 \times 10^8$, the NTV torque density (dashed line) is strongly reduced by the plasma response compared to the vacuum field result (solid). For $S_0 = 0.53 \times 10^8$, the magnitude of the NTV torque density (dashed dotted line) is larger than the observed one. The magnitude of the NTV torque density for $S^0 = 0.8 \times 10^8 8$ (dotted line) is very close to the observed one.

The displacement near the plasma core calculated using the vacuum field assumption is around 5.2cm for 1.4kA perturbation current applied in this experiment, while the result from the MHD response is about 0.9 cm for $S_0 = 1.1 \times 10^8$ and 1.6 cm for $S_0 = 0.8 \times 10^8$. It can be used to test the plasma response model by comparing this displacement with the observation.

3.5. ESTIMATION OF THE N = 1 DISPLACEMENT ON JET

It is generally very difficult to directly measure the 3D displacement. To measure the n = 1 displacement, we need at least two measurements of the plasma position at different toroidal positions simultaneously. There are two arrays of the Soft-X-Ray diagnostics with a vertical view located at different toroidal position on JET [34]. The difference in the toroidal angle of these two arrays is 135 degree. One of them is located at the toroidal position with maximum magnetic perturbation in the R direction. The distance between the adjacent chords at the mid-plane for each array is about 5cm. The shift of the peak position in the emission profile measured from each array can be roughly an estimation of the displacement of the magnetic axis, although it is a line-integrated signal. The similarity and difference between these two shifts can be used as the estimations of the n = 0 and n = 1 components of the displacement in the major radius direction.

The displacement during the application of the magnetic perturbation obtained from this method are shown in Fig.19. The reference time is chosen at t = 18.6s, which is just before the application of the perturbation. The obtained n = 0 displacement (middle), which is caused by the pick-up of the perturbation field in the magnetic signals for the plasma position control, are around 5cm and

are in good agreement with that from the equilibrium reconstruction. There is a clear difference in the evolution of the n = 0 (middle) and n = 1 (top) components of the displacement. The n = 1 displacement depends almost linearly on the perturbation current during both the coil current ramp-up and ramp-down phases.

Figure 20 shows the dependence of the displacement on the perturbation coil current during the current ramp-up phase. They show a good linear dependence, which suggests a linear plasma response. The displacement estimated from this method is around 1cm for 1.4kA coil current by the fitting of the data from these 6 pulses. It is close to the result from the MHD response with $S_0 = 1.1 \times 10^8$, and it is about half of the displacement required for good agreement between the magnitude of the NTV torque and the observed one.

With this value of the displacement, the NTV torque is about a factor of 22 = 4 times smaller than the observed one. If we use the displacement estimated from the Pulse No: 77329, the difference can be further reduced to about a factor of $1.52 \approx 2$. The agreement between the magnitude of the NTV torque and the observed one is improved compared to the result from the vacuum field assumption. This result suggests the importance of the accurate modeling and measuring of the plasma response in the NTV torque evaluation.

3.6. NTV MODELING ON TEXTOR

The NTV torque density calculated using the vacuum field assumption on TEXTOR is shown in Fig.21. In both the resonant and non-resonant cases, the NTV torque density is very small. The NTV torque density near the plasma core for the resonant one is about 4 orders smaller than that on JET, because of the fast decay of the perturbation field inside the plasma in this coil configuration, which is shown in Fig.8. The angular momentum density on TEXTOR are in the same order as that on JET. Therefore, this torque has a negligible effect on the plasma rotation on TEXTOR. This result agrees with the observation that there is no braking effect from the n = 2 DED on TEXTOR.

SUMMARY AND CONCLUSION

The non-resonant magnetic braking effect induced by an Non-Axisymmetric Magnetic Perturbation (NAMP) is investigated on JET and TEXTOR in this paper.

The collionality dependence of the torque induced by the n = 1 NAMP generated by the EFCCs on JET is observed . The observed torque is located mainly in the plasma core (normalized $\rho < 0.4$) and increases with decreasing collisionality.

The NTV torque in collisionless regime is modeled by using the numerical solution of the bounce averaged drift kinetic equation. The calculated collisionality dependence of the NTV torque is in good agreement with the experimental observation on JET. The reason for this collisionality dependence is that the torque in the plasma core on JET mainly comes from the contribution of the trapped electron, which is still in the $1/\nu$ regime. The trapped electron flux is normally neglected in the past studies. However, it really gives the dominant contribution in the plasma core on JET.

The strongest NTV torque on JET is also located near the plasma core.

The magnitude of the NTV torque strongly depends on the plasma response, which is also discussed in this paper. The observed torque is about one order smaller than the NTV torque evaluated using the vacuum field assumption. The plasma response is important for the NTV torque evaluation. It is very sensitive to the plasma resistivity in the linear MHD response model used in this paper. The magnitude of the NTV torque density is very close to the observed one, if we choose the Lundquist number at the plasma core about $S_0 = 0.8 \times 10^8$.

The NTV torque density near the plasma core is mainly determined by the m/n = 1/1 displacement. In this experiment, the displacement near the plasma core evaluated using vacuum field assumption is about 5.2cm, while the result from the MHD response is only about 1.6 cm for $S_0 = 0.8 \times 10^8$. The displacement estimated from the three-dimensional shift of the peak positions of the Soft-X-Ray emission has a good linear dependence on the applied perturbation current and is around 1 cm for the applied maximum current in this experiment. With this displacement, the calculated NTV torque is about a factor of 22 = 4 times smaller than the observed torque. The agreement between the magnitude of the observed torque and the NTV torque is also improved when this plasma response is taken into account, compared to the results using the vacuum field assumption.

There is no obvious braking effect with n = 2 NAMP generated by the DED on TEXTOR. The calculated NTV torque for this coil configuration on TEXTOR is also very small.

The observations on JET and TEXTOR also suggest that the non-resonant magnetic braking effect strongly depends on the coil configuration. To avoid the non-resonant magnetic braking, the perturbation field near the plasma core should be reduced. Therefore, the coils should be located as close as possible to the plasma or we should use a relatively high n number, so that the field has a fast decay along the minor radius to the plasma core.

Besides the complexity in the NTV theory itself, it is shown that the plasma response is another essential issue for the NTV torque calculation. In the present results, the biggest uncertainty part is the plasma response. To increase the accuracy in the NTV torque evaluation in the future work, it is necessary to improve the modeling of the plasma response and the measurement of the 3D displacement in the experiment. This could be a big challenge for both plasma theory and experiment. The study in this topic is still in progress.

ACKNOWLEDGMENTS

This work was supported by EURATOM and carried out within the framework of the European Fusion Development Agreement. The views and opinions expressed herein do not necessarily reflect those of the European Commission. Additional support from the Helmholtz Association in frame of the Helmholtz-University Young Investigators Group VH-NG-410 is gratefully acknowledged. One of the authors, Y. Sun, would like to acknowledge the support from the National Natural Science Foundation of China under Grant No. 10725523.

REFERENCES

[1]. T. Evans et al, Physical Review Letters **92**, 235003 (2004).

[2]. Y. Liang et al, Physical Review Letters **98**, 265004 (2007).

[3]. E.J. Strait et al , Physics of Plasmas **11**, 2505 (2004).

[4]. W. Zhu et al, Physical Review Letters **96**, 225002 (2006).

[5]. A.M. Garofalo et al, Physical Review Letters **101**, 195005 (2008).

[6]. H. Reimerdes et al, Nuclear Fusion **49**, 115001 (2009).

[7]. S.A. Sabbagh et al, Nuclear Fusion 50, 025020 (2010).

[8]. Y. Sun et al, Plasma Physics and Controlled Fusion **52**, 105007 (2010).

[9]. K.C. Shaing, Physics of Plasmas **10**, 1443 (2003).

[10]. A.J. Cole C.C. Hegna, J.D. Callen, Physical Review Letters **99**, 065001 (2007).

[11]. M.Bécoulet et al, Nuclar Fusion **49**, 085011 (2009).

[12]. M.D. Hua et al, Plasma Physics and Controlled Fusion **52**, 035009 (2010).

[13]. Y. Liang et al, Nuclear Fusion **50**, 025013 (2010).

[14]. K.C. Shaing et al, Physics of Plasmas **15**, 082506 (2008).

[15]. K.C. Shaing S.A. Sabbagh, M.S. Chu, Plasma Physics and Controlled Fusion **51**, 035009 (2009).

[16]. K.C. Shaing S.A. Sabbagh, M.S. Chu, Nuclear Fusion **50**, 025022 (2010).

[17]. J.-K. Park A. H. Boozer, J.E. Menard, Physical Review Letters **102**, 065002 (2009).

[18]. Y. Sun et al, Physical Review Letters **105**, 145002 (2010).

[19]. Y. Sun et al, Nuclear Fusion **51**, 053015 (2011).

[20]. K.C. Shaing et al, Nuclear Fusion **50**, 125008 (2010).

[21]. K.C. Shaing et al, Nuclear Fusion **51**, 073043 (2011).

[22]. Y. Liang et al, Physical Review Letters **105**, 065001 (2010).

[23]. K. H. Finken et al, Nuclear Fusion **39**, 637 (1999).

[24]. K. H. Finken et al, Physical Review Letters **94**, 015003 (2005).

[25]. J.-K. Park et al, Physics of Plasmas **16**, 056115 (2009).

[26]. K.C. Shaing, Physical Review Letters **87**, 245003 (2001).

[27]. M.F. Heyn et al, Nuclear Fusion **46**, S159 (2006).

[28]. Q. Yu et al, Nuclear Fusion **48**, 024007 (2008).

[29]. E. Nardon et al, Nuclear Fusion **50**, 034002 (2010).

[30]. Y. Liu et al, Physics of Plasmas **17**, 122502 (2010).

[31]. Y. Liu et al, Nuclear Fusion **51**, 083002 (2011).

[32]. M.J. Lanctot et al, Physics of Plasmas **17**, 03071 (2010).

[33]. M.P. Gryaznevich et al, Plasma Physics and Controlled Fusion **50**, 124030 (2008).

[34]. B. Alper et al, Review of Scientific Instruments **68**, 778 (1997).

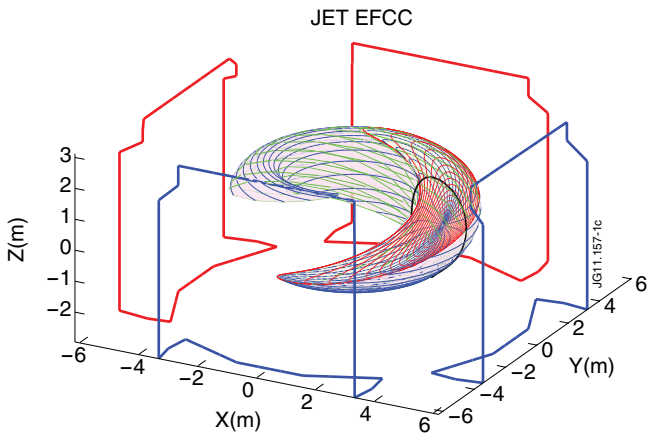

Figure 1: The Error Field Correction Coils (EFCCs) and the equally spaced Hamada coordinates for half torus of the plasma configuration on JET.

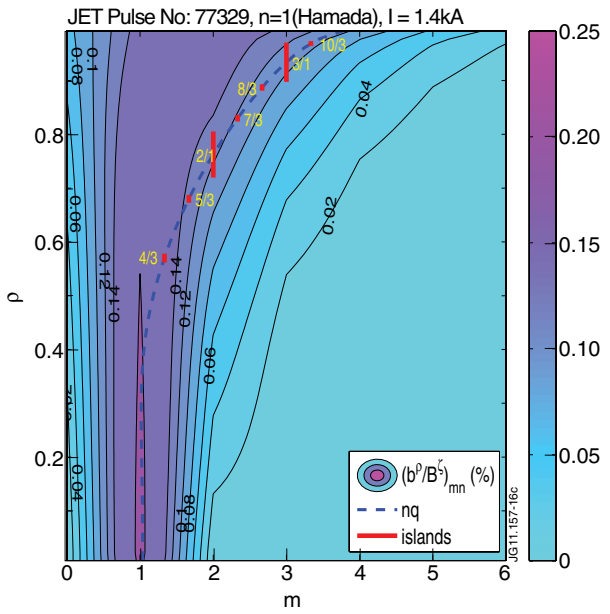

Figure 2: The strength of the n = 1 component of the RMP spectrum in Hamada coordinates $(b^{\rho}/B^{\zeta})_{mn}(\%)$ for JET Pulse No: 77329, the resonance condition m = nq (dashed line) and the locations and widths of the islands (shot solid lines marked on each rational surface) induced by the NAMP using the vacuum field assumption.

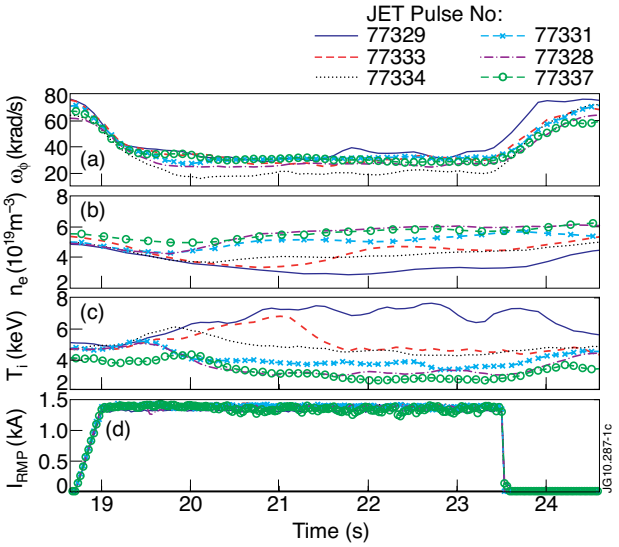

Figure 3: The temporal evolution of the plasma rotation (A), density (B), ion temperature (C) at R_0 = 3.0m (near the magnetic axis) during the application of n = 1 NAMP field (D) for a series of pulses where the densities were restored at different levels.

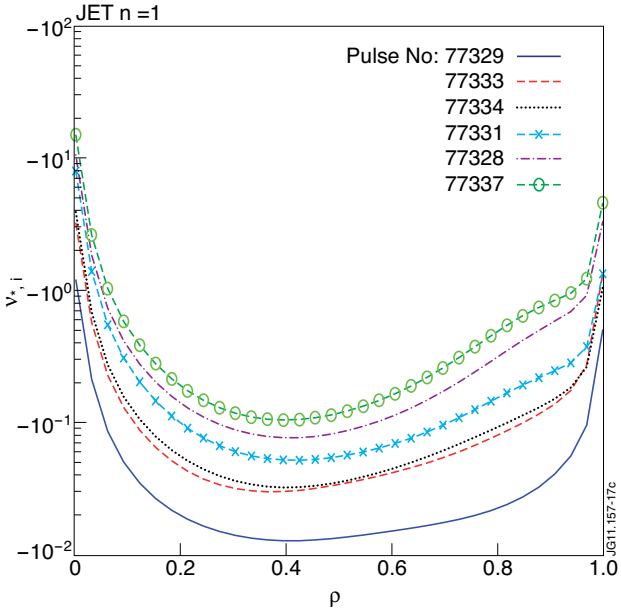

Figure 4: The profiles of the effective collisionality.

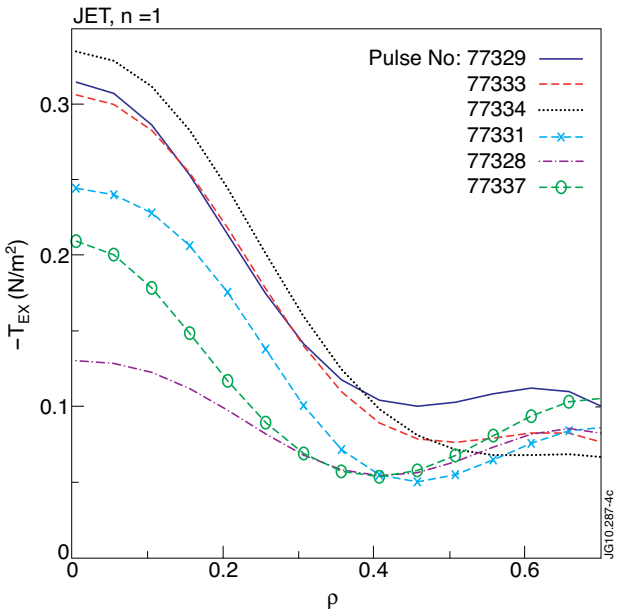

Figure 5: The observed torque density profiles induced by NAMP.

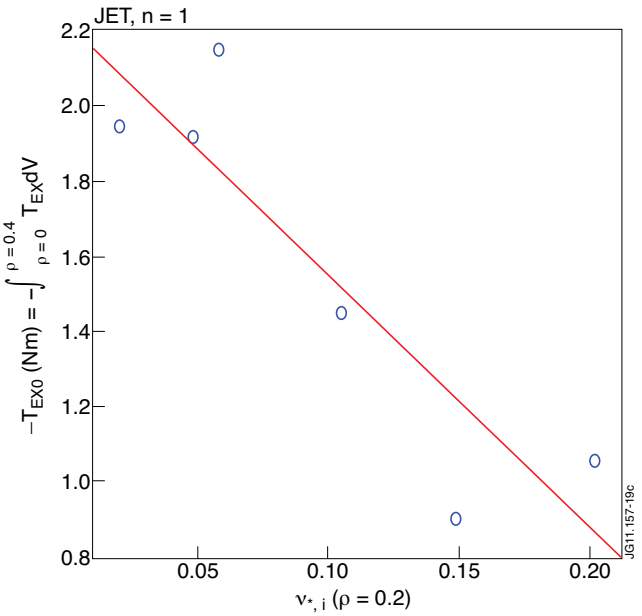

Figure 6: The dependence of the observed total torque inside the ρ = 0.4 surface on the collisionality.

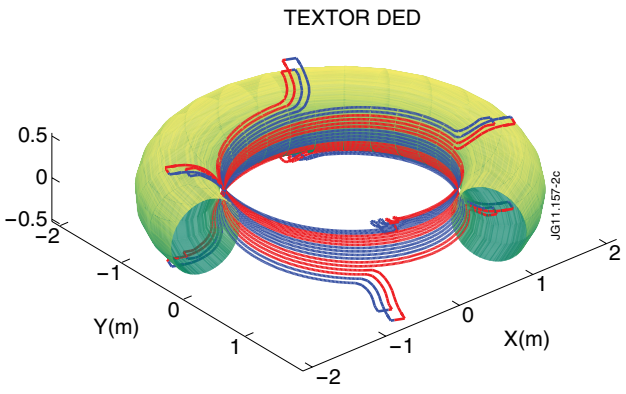

Figure 7: The Dynamic Ergodic Divertor (DED) coils on TEXTOR.

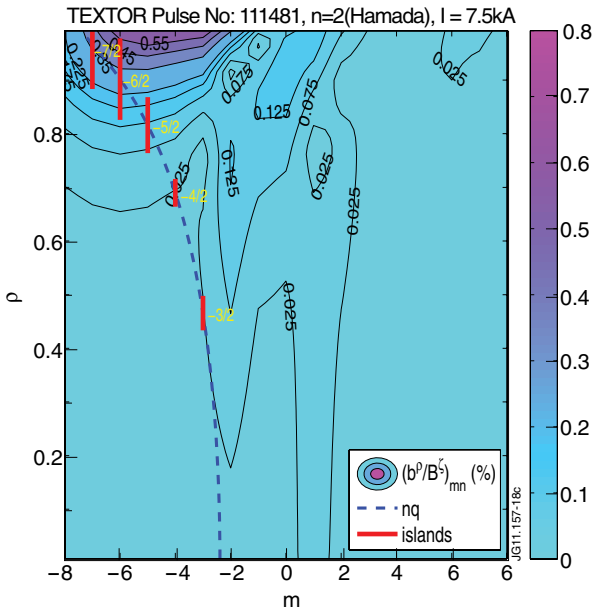

Figure 8: The RMP spectrum of the n = 2 DED coil configuration on TEXTOR.

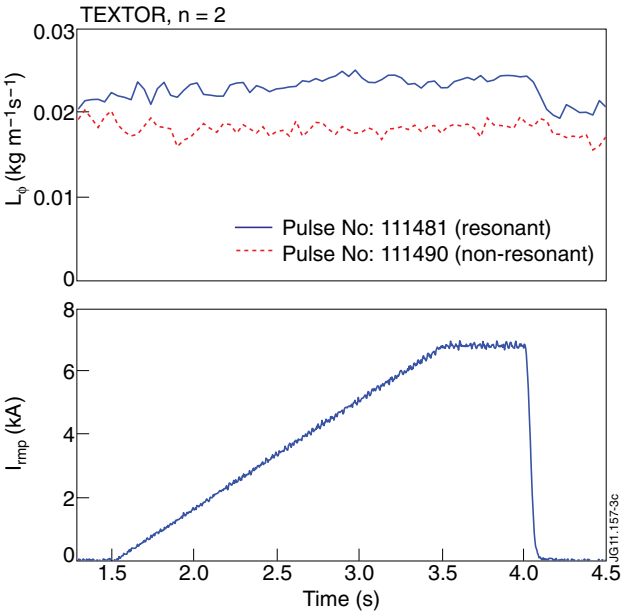

Figure 9: The evolution of the toroidal angular momentum density $L_\phi = N_i M_i R_0^2 \omega_\phi$ near the plasma core for both resonant (solid line, top) and non-resonant (dashed line, top) configurations with the DED coil current (bottom).

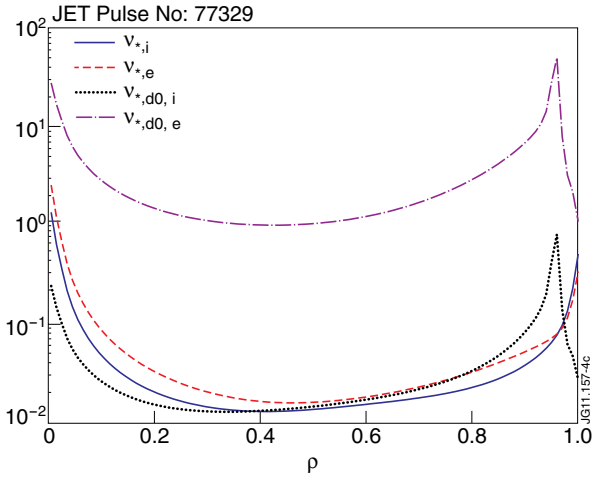

Figure 10: The profiles of the normalized collisionalities $\nu_{*,i}$ (solid), $\nu_{*,e}$ (dashed), $\nu_{*d0,i}$ (dotted), and $\nu_{*d0,e}$ (dashed dotted).

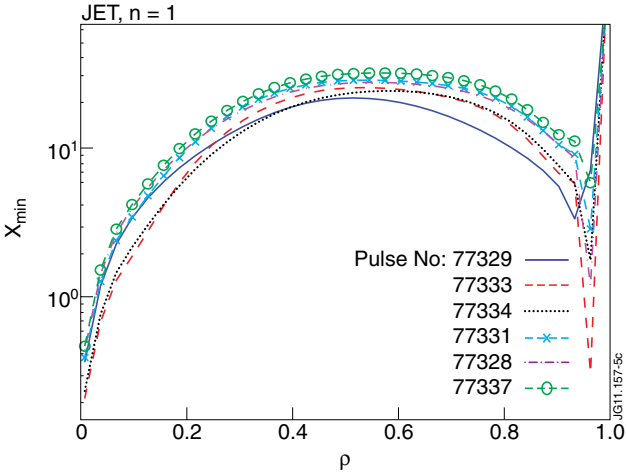

Figure 11: The profiles of $x_{min} \equiv |/q\omega_E/\omega_{B0}|$ for different pulses.

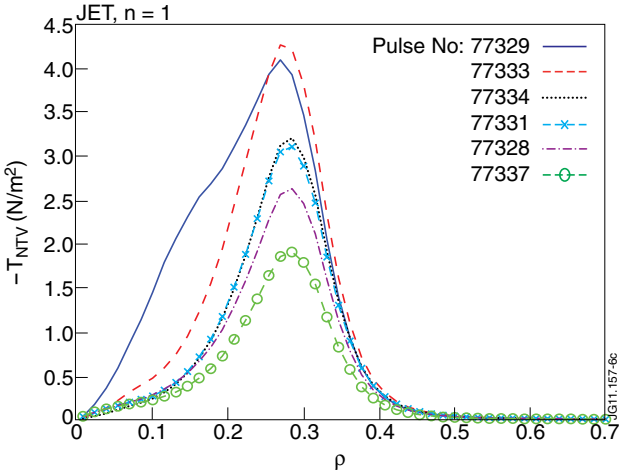

Figure 12: The NTV torque density profiles on JET calculated with the vacuum field assumption.

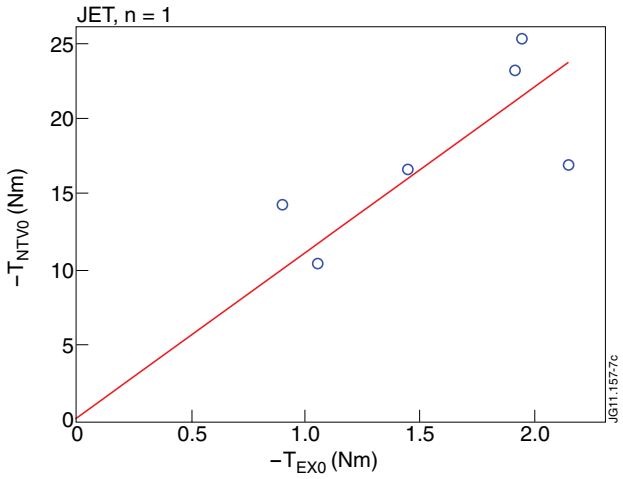

Figure 13: Comparison between the observed torque and the NTV torque inside ρ = 0.4 surface.

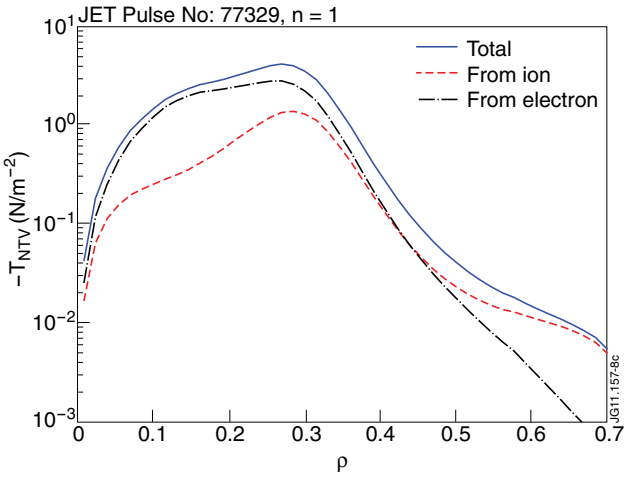

Figure 14: The NTV torque density contributed from ion (dashed line) and electron (dashed- dotted line).

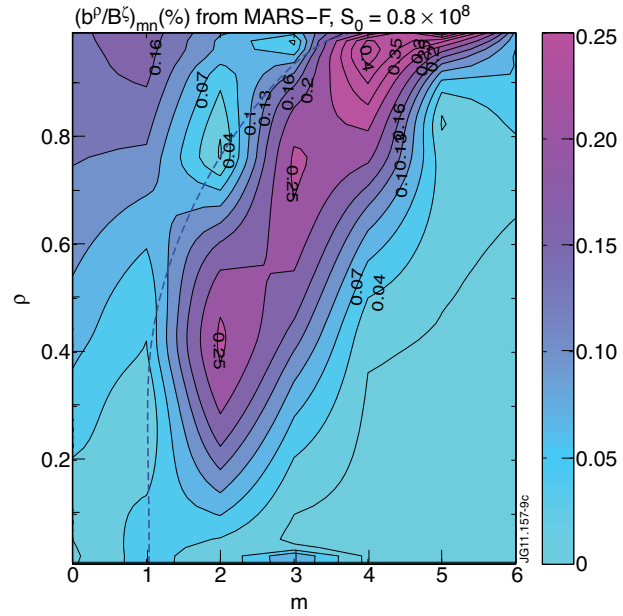

Figure 15: The spectrum of the magnetic perturbation with plasma response with $S_0 = 0.8 \times 10^8$ for the same pulse shown in Fig. 2. The dashed line indicates the resonance condition $m - nq = 0$.

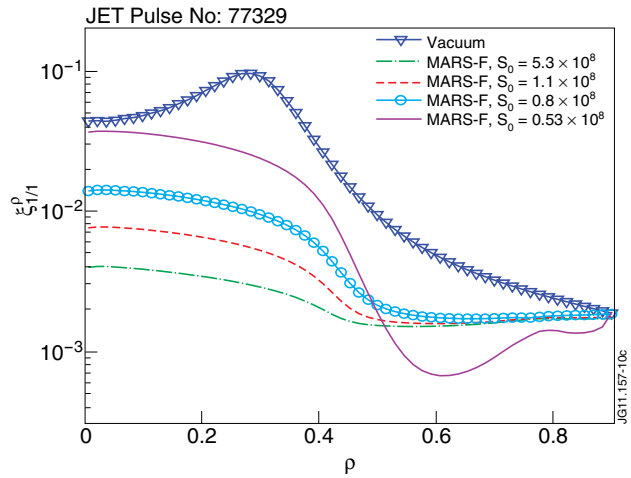

Figure 16: The m/n = 1/1 component of the radial displacements calculated using the vacuum field assumption(triangles) and the MHD response with $S_0 = 5.3 \times 10^8$ (dashed dotted), 1.1×10^8 (dashed), 0.8×10^8 (circles), and 0.53×10^8 (solid).

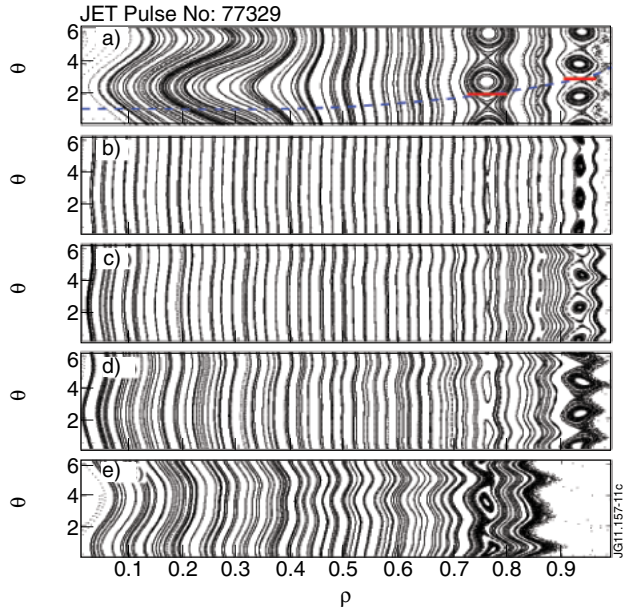

Figure 17: The Poincaré plot of the magnetic field with magnetic perturbation calculated using the vacuum field assumption(A) and the MHD response with S_0 = 5.3 × 10^8 (B), 1.1 × 10^8 (C), 0.8 × 10^8 (D), and 0.53 × 10^8 (E).

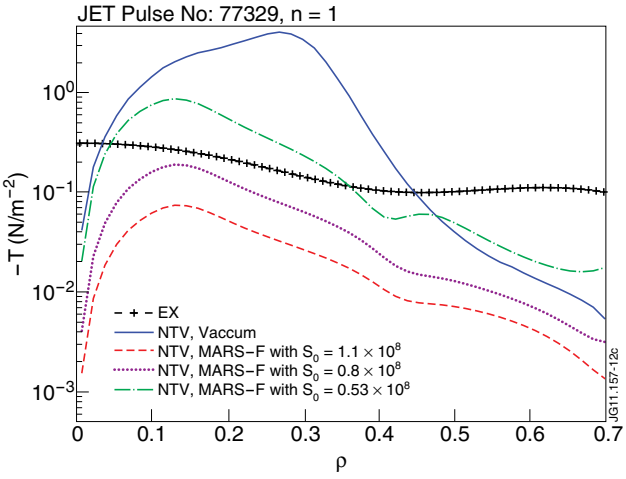

Figure 18: The NTV torque density evaluated using the perturbation field with the vacuum field assumption (solid) and with MHD response modeled from the MARS-F code for S_0 = 1.1 × 10^8 (dashed), 0.8 × 10^8 (dotted), and 0.53 × 10^8 (dashed dotted), compared to the experimentally observed one (+).

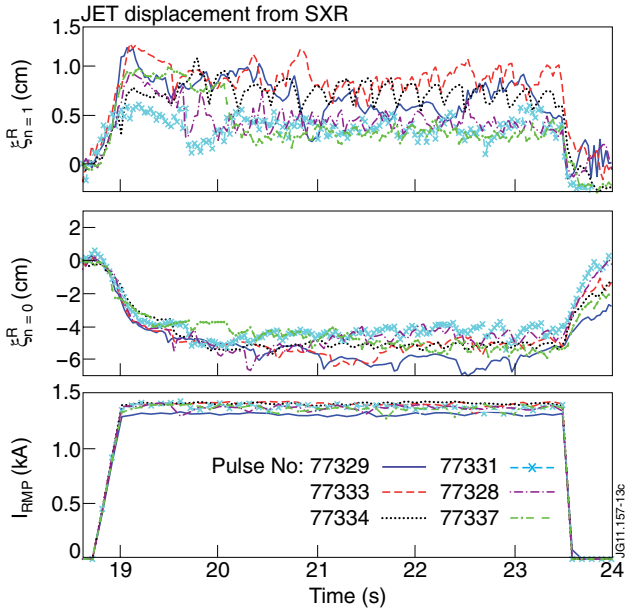

Figure 19: The evolution of the n = 1 three-dimensional displacement (top) and the n = 0 two- dimensional displacement (middle), estimated from the shift of the peak position of the Soft-X-Ray emission, with the Error Field Correction Coil current (bottom).

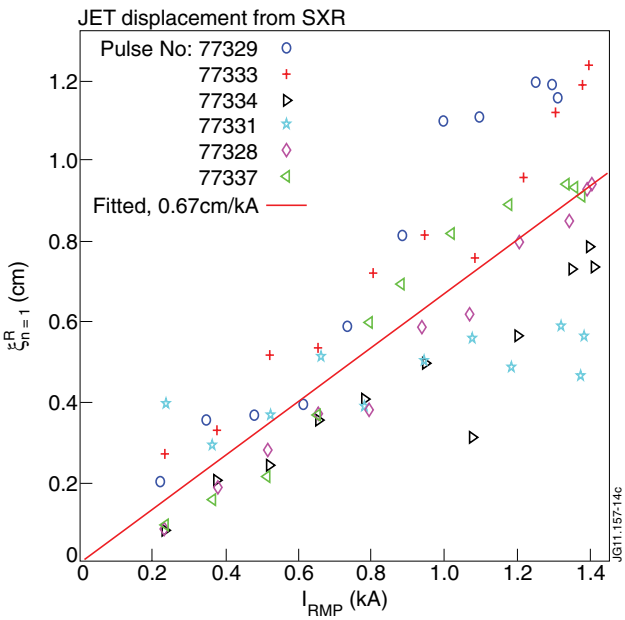

Figure 20: The dependence of the n = 1 displacement on the coil current. The solid line is fitted from the estimated n = 1 displacements of the six JET pulses.

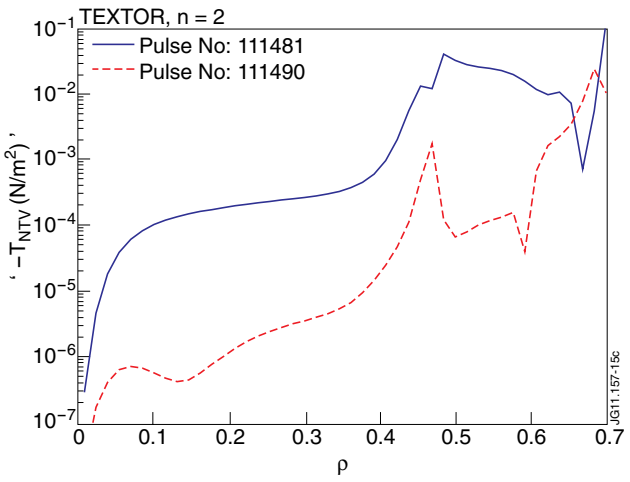

Figure 21: The NTV torque density profiles on TEXTOR calculated using the vacuum field assumption.